Resistively detected NMR in a triple-gate quantum point contact: Magnetic field dependence

Annisa Noorhidayati,[1] Mohammad Hamzah Fauzi,[2,3] Muhammad Fauzi Sahdan,[1,*] Shunta Maeda,[1] Ken Sato,[1] Katsumi Nagase,[1] and Yoshiro Hirayama[1,2,4,†]

[1]*Department of Physics, Tohoku University, Sendai 980-8579, Japan*
[2]*CSRN, Tohoku University, Sendai 980-8577, Japan*
[3]*Research Center for Physics, Indonesian Institute of Sciences, South Tangerang City, Banten 15314, Indonesia*
[4]*CSIS (Core Research Cluster), Tohoku University, Sendai 980-8577, Japan*

(Received 20 August 2019; revised manuscript received 10 October 2019; published 28 January 2020)

We report a resistively detected nuclear magnetic resonance (RDNMR) measurement in a GaAs-based quantum point contact in the quantum Hall breakdown regime. We focus on the detection of the ^{75}As RDNMR signal at different perpendicular magnetic fields in the presence of electrons occupying the lowest Landau level. We confirm successful RDNMR detection down to $B = 1.25$ T ($B = 3.5$ T) using a high-mobility (low-mobility) device. All the RDNMR signals exhibit a threefold spectra attributed to electric quadrupole interaction. We find that the separation between the central transition and its satellite, $\Delta_f \approx 20$ kHz, remains unaffected by magnetic-field variation. Interestingly, the central NMR linewidths vary with the field strength. Above $B = 3$ T, the linewidth tends to saturate around 13 kHz. Below $B = 3$ T, the linewidth decreases in proportion with field and approaches a lower limit of 1 kHz corresponding to the GaAs nuclear dipole interaction as the field decreases to $B = 1.25$ T.

DOI: 10.1103/PhysRevB.101.035425

I. INTRODUCTION

When a two-dimensional electron gas (2DEG) is subjected to a perpendicular magnetic field at low temperatures, it exhibits several interesting phenomena. One of them is the integer quantum Hall effect (IQHE) characterized by the formation of Landau level (LL) bands [1]. The general features of the IQHE include a smoothly connected series of quantized conductance in units of $G_0 = \frac{2e^2}{h}$, observed at zero magnetic field in the quantum point contact (QPC) [2–4]. In the QPC we can easily control the potential shape of the confinement in the saddle point by changing the bias voltages applied to the gates of the QPC device [3,5,6]. For example, the position of the IQHE conductance plateau can be controlled in the QPC, under a perpendicular magnetic field.

Nonzero nuclear spin polarization and its resistive detection enable resistively detected NMR (RDNMR) in semiconductor quantum systems, particularly in those based on GaAs. The interaction between the electron and nuclear spins (hyperfine interaction) leads to a change in the conductance, and the high sensitivity enables RDNMR measurement in a single quantum well [7–10] unveiling many interesting phenomena in two-dimensional systems [11–14]. RDNMR studies have been extended to one-dimensional systems and/or QPCs [15–17]. We exploit the QPC ability to locally control the saddle potential shape and manipulate the dynamic nuclear spin polarization (and its detection) in the narrow channel to understand the RDNMR characteristics in QPCs [18,19]. Although the effect of dynamic nuclear spin polarization on QPC transport has been well established, there is no direct experimental study on the limitations of RDNMR detection, including the comparison between high-mobility and low-mobility devices, and how the central transition linewidth, which supposedly reflect the electronic distribution in the point contact, evolve with fields. Thanks to a large quadrupole splitting, the central NMR linewidth is free from strain-induced linewidth broadening. The linewidth solely depends on nuclear dipolar coupling and electron distribution. While the former is field independent, the latter is thought to depend on the field, a manifestation of electron-electron interaction in the system.

II. DEVICE AND METHOD

In this study we first systematically test the condition limiting the observability of the RDNMR signal, under the simplest possible condition where the lowest LL alone ($N = 0$) is occupied. The electron density in a quantum well is adjusted by applying the backgate bias (V_{BG}) to maintain this condition for all the given magnetic fields. We decrease the magnetic field and observe the changes in the RDNMR signal. By doing so, we can track the evolution of RDNMR spectra from high to the lowest possible magnetic field. High-mobility (low-mobility) Hall bar-shaped AlGaAs/GaAs/AlGaAs quantum well wafers are used in this study. A 20-nm quantum well is located at 175 nm (140 nm) from the surface. The electron mobility is $\mu = 1.47 \times 10^6$ cm^2 V s ($\mu = 2.8 \times 10^5$ cm^2 V s) at $n_s = 1.8 \times 10^{11}$ cm^{-2}. The photolithography technique is employed to cut the wafer into a 30-μm wide and 100-μm long Hall bar. In this experiment, we use a triple-gate QPC consisting of a split-gate pair and an additional center gate

*Present address: Department of Physics, National University of Singapore, Singapore 117551, Singapore.
†yoshiro.hirayama.d6@tohoku.ac.jp

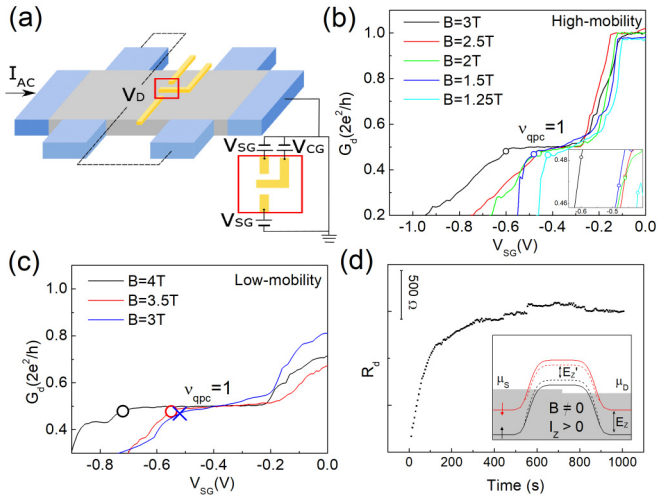

FIG. 1. (a) Schematic of the device mounted on a 300-mK cryostat. The QPC includes triple Schottky gates consisting of a pair of split gates and an additional center gate. An excitation current $I_{AC} = 1$ ($I_{AC} = 10$) nA is applied for transport (RDNMR) detection. (b) and (c) Conductance profiles of high-mobility and low-mobility devices as a function of the split-gate voltage at various magnetic fields, respectively. The white circle (cross mark) denotes the point of successful (failed) RDNMR detection. (d) Diagonal resistance trace throughout the current-induced dynamic nuclear polarization (DNP) process prior to RDNMR detection. The inset shows the potential barrier sensed by the conduction electrons, which is modified by nuclear spin polarization.

patterned by evaporating 5-nm Ti/20-nm Au on top of the Hall bar as schematically depicted in Fig. 1(a). The nominal length of the QPC channel is 600 nm. The width of the center gate is 200 nm, and the separation between the center and side gates is also 200 nm. Negative voltage is applied to the split gates (V_{SG}) to confine the electron in the quasi-one-dimensional channel, while the bias applied to the center gate (V_{CG}) modifies the shape of the confinement potential. A coil wrapped around the sample provides an rf magnetic field parallel to the sample, for NMR measurements. We conduct transport and RDNMR measurements in a single shot ^{3}He refrigerator with a base temperature of 300 mK. We monitor the diagonal conductance using a Lakeshore 370 AC resistance bridge. Here we control the outside/bulk filling factor (ν_b) and the inside/QPC filling factor (ν_{qpc}) under the simplest combination $(\nu_b, \nu_{qpc}) = (2, 1)$, which is the contribution of the (lowest Landau level) alone. Figure 1(a) shows the device layout and experimental setup (rf coil not shown), which is similar to the setup used in Ref. [18].

III. RESULTS

We apply $I_{AC} = 1$ nA to measure the conductance profile of the QPC. To maintain $\nu_b = 2$ for any given magnetic field, higher electron density is required at higher magnetic fields. At $B = 1.25$ T (3 T), $\nu_b = 2$ corresponds to $n_s = 6.045 \times 10^{10}$ cm^{-2} ($n_s = 1.451 \times 10^{11}$ cm^{-2}). Therefore, V_{BG} is tuned to set $\nu_b = 2$ for a given magnetic field. The V_{SG} pinch-off voltage becomes more negative at a higher magnetic field due to the higher electron density as expected. We have an additional center gate in our QPC. Applying a more positive (negative) center-gate bias V_{CG} at a fixed electron density deepens (shallow) the confinement potential and increases the separation between the subbands, resulting in a more negative (positive) pinch-off voltage [20]. In our experiment, we set the inside of the QPC at ν_{qpc} by controlling both V_{CG} and V_{SG}. We adjust V_{CG} such that the plateau is centered around the same V_{SG} value for all the magnetic fields. This retains the RDNMR detection point around the same V_{SG}. For example, $V_{CG} = -0.2$ V is applied at $B = 3$ T and $V_{CG} = -0.1$ V is applied at $B = 1.25$ T. Figure 1(b) [1(c)] shows the conductance profile of a high-mobility (low-mobility) device under the above mentioned conditions.

Although the plateau appears in the same V_{SG} range, other noticeable effects of the magnetic field such as the quality of the $\nu_{qpc} = 1$ conductance plateau can be observed. The magnetic field (B) changes the separation energy between the subbands and lifts the spin degeneracy due to Zeeman energy ($E_Z = g^*\mu_B B$). Increasing the magnetic field results in higher separation between the up-spin and down-spin channels. As the Zeeman separation becomes more notable in proportion with B, a longer and more pronounced $\nu_{qpc} = 1$ plateau can be observed. Using a high-mobility device, we observe the $\nu_{qpc} = 1$ plateau down to $B = 1.25$ T, whereas with a low-mobility device, the $\nu_{qpc} = 1$ plateau become imperceptible at $B = 3$ T. This is because the broader density of states of the electron LLs in a low-mobility wafer require higher B to clearly separate both energetically and spatially the two different spin states.

As the RDNMR-signal shape and strength are sensitive to the detection point [18,21–23], we carefully select the RDNMR detection point at around the same value of $\nu_{qpc} < 1$, denoted by the white circles in Figs. 1(b) and 1(c). Prior to RDNMR detection, we polarize the nuclear spin through a current induced-dynamic nuclear polarization (DNP) process by applying 10-nA AC current at the off-resonance frequency for 1000 s. The diagonal resistance (R_d) attains a constant value after a few hundred seconds as shown in Fig. 1(d), indicating that the nuclear spin polarization is saturated in the channel. Applying a bias current higher than the critical current of the IQHE breakdown excites electrons to the upper LLs accompanied by electron spin flip. When the electrons in the up-spin channel are scattered to the down-spin channel, they can transfer their polarization to the nuclear spins (flip-flop process) through hyperfine interaction and build positive nuclear polarization [18,24,25]. The slowly evolving R_d over time is evidence of the DNP process [17]. The timescale of the nuclear spin polarization is in good agreement with previous reports on GaAs devices [7,8,26].

The RDNMR detection mechanism is depicted in the inset of Fig. 1(d). The potential barrier sensed by the up-spin and down-spin electrons is separated by the Zeeman energy E_Z (see solid lines). In the presence of positive nuclear polarization (positive indicates that the nuclear polarization is parallel to the external magnetic field B), the Zeeman separation decreases to $E'_Z = g^*\mu_B(B + B_N)$ with respect to the Overhauser shift (see the dashed lines). It is noteworthy that B_N becomes negative, in the case of positive nuclear polarization. As the conductance through the QPC is sensitive to small changes in the barrier, nuclear polarization can be

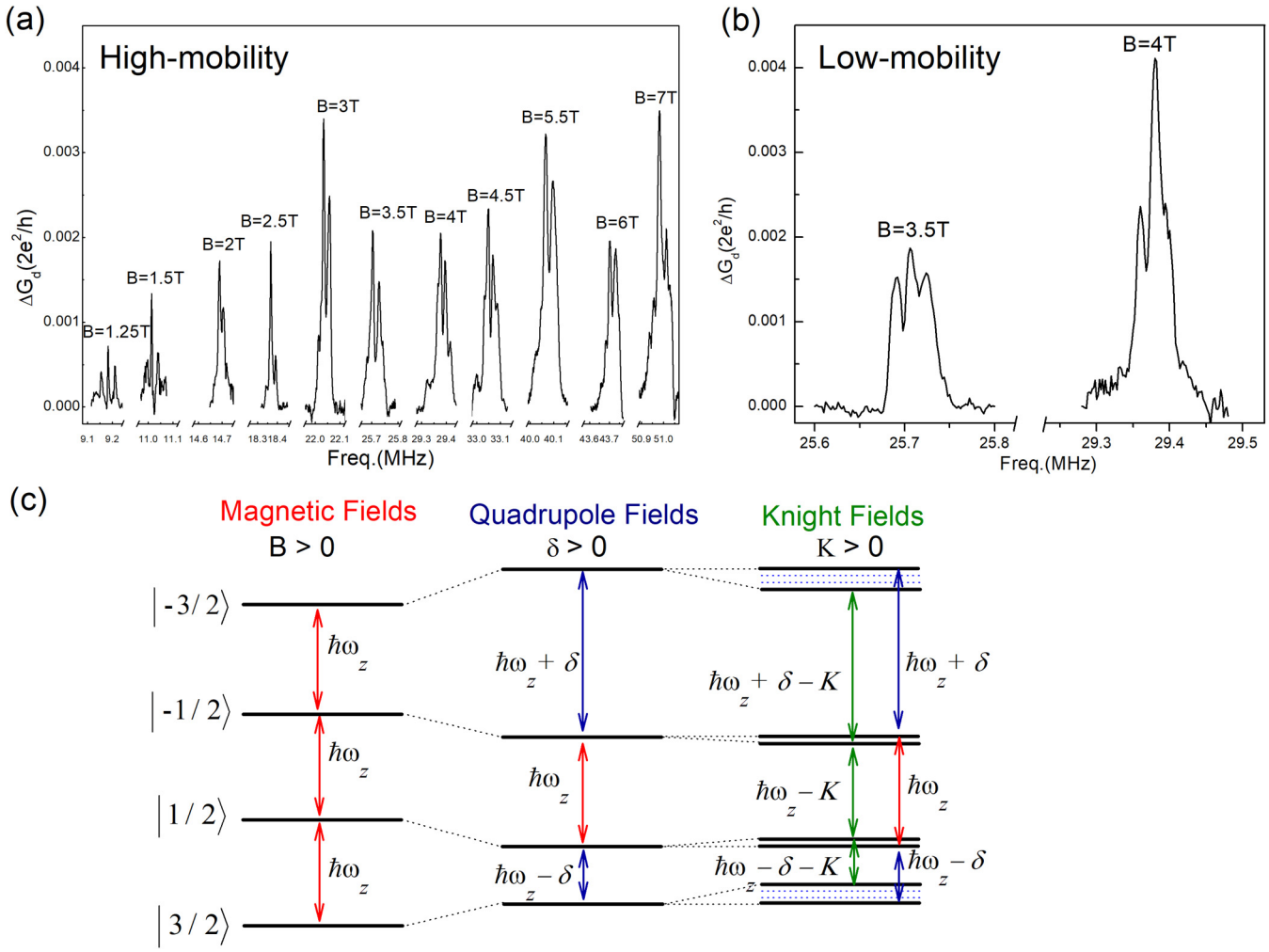

FIG. 2. (a) and (b) RDNMR signals of the high-mobility and low-mobility devices measured at $\nu_{qpc} < 1$ with magnetic-field variation. The strain around the QPC structure increases the quadrupolar fields, resulting in a threefold degeneracy spectra for all the RDNMR signals. (c) Energy diagram of an $I = \frac{3}{2}$ nuclear spin system in the presence of external magnetic fields (left), quadrupole fields (middle), and Knight fields (right).

sensitively detected by determining the QPC conductance. At $\nu_{qpc} < 1$, the up-spin electrons alone pass through the channel, whereas the down-spin ones are completely blocked. Therefore, the barrier for the up-spin electrons determines the QPC conductance.

After the DNP process, we detect the RDNMR by rf sweeping near the ^{75}As Larmor frequency at a sweep rate of 100 Hz/s. At the corresponding frequency, the nuclear spins are depolarized by the rf-magnetic field [9] and the potential barrier reverts to its original value separated by E_Z. The up-spin electrons sense a decrease in the potential barrier, and the transmission increases [18,19]. Consequently, we detect the conductance peaks in the G_d trace as shown in Figs. 2(a) and 2(b), where the RDNMR signals detected at several B are summarized for both high- and low-mobility devices. The frequency of the RDNMR signal varies linearly with respect to the applied magnetic field, confirming that all the signals are at the Larmor frequency of ^{75}As. We detect the RDNMR signal down to $B = 1.25\,\mathrm{T}$ ($B = 3.5\,\mathrm{T}$) using a high-mobility (low-mobility) device. The signal-to-noise ratio (SNR) is forfeited as B decreases.

The RDNMR signal strength is proportional to the degree of nuclear spin polarization, which is enhanced by electron scattering between different spin edge channels in the IQHE breakdown regime. Here we can observe that the amplitude of the RDNMR signal decreases when the applied magnetic field is reduced. This decrease in the magnetic field renders the separation between the up-spin and down-spin channels ambiguous, thereby reducing the spin-flip scattering probability and incorporating a smaller number of spins in the RDNMR detection process. It is noteworthy that the successful detection of the RDNMR signal coincides well with the clear observation of the $\nu_{qpc} = 1$ plateau. However, it is not solely dependent on the Zeeman-splitting separation. The limitation of the ohmic contacts also plays an important role in delimiting the RDNMR observability in our experiment. The electron density is lesser when the magnetic field is decreased by reducing $V_{BG} = 0.8\,\mathrm{V}$ ($B = 3\,\mathrm{T}$) to $V_{BG} = -0.9\,\mathrm{V}$ ($B = 1.25\,\mathrm{T}$) for tuning $\nu_b = 2$. At this point, the electron density is close to the lowest density to obtain good ohmic contacts and reliable transport characteristics. It is difficult to make electron density, i.e., magnetic field, much lower.

The ^{75}As nuclear spin has a spin number $I = \frac{3}{2}$, and the magnetic quantum number may take values $|m\rangle = |+\frac{3}{2}\rangle$, $|+\frac{1}{2}\rangle$, $|-\frac{1}{2}\rangle$, $|-\frac{3}{2}\rangle$, providing four different energy states as illustrated in Fig. 2(c). All nuclear state with spin number $I > \frac{1}{2}$ have nonspherical charge distribution and a nonzero electric quadrupole moment (Q). This quadrupole moment can interact with electric field gradient (EFG) induced by strain and shifts the energy-levels separation. In the absence of electric field gradient, all four states are equidistant in energy ($\hbar\omega_Z$), and present a single NMR signal for any $\Delta m = \pm 1$ transition as indicated by the leftmost energy level diagram in Fig. 2(c). In the presence of additional quadrupole interaction, without considering the multiple photon process [27], this single peak spectrally splits into three different peaks [9,14] with the energy separation modified by $\pm\delta$ as illustrated by the middle energy-level diagram in Fig. 2(c). In a perfectly uniform electric field gradient, it only splits the resonance without introducing additional broadening. The first, second, and third peaks correspond to $(|-1/2\rangle \leftrightarrow |-3/2\rangle)$, $(|+1/2\rangle \leftrightarrow |-1/2\rangle)$, and $(|+3/2\rangle \leftrightarrow |+1/2\rangle)$, respectively. The first and third peaks are attributed to satellite transitions (STs) in which the spectral position is modified by quadrupole interaction (δ), whereas the second peak is attributed to the central transition (CT) and is not modified by quadrupole interaction. The rightmost energy level diagram in Fig. 2(c) depicts the shifts in energy levels and resonance frequency due to the Knight shifts (K). The presence of electron spin polarization changes the effective magnetic field felt by the nuclear spin. Since the electron density is spatially distributed, the Knight shift felt by the nuclear spin would vary in space and can be observed as an inhomogeneous broadening in the resonance peaks.

All the RDNMR signals in Figs. 2(a) and 2(b) show threefold spectra with a separation of $\Delta_f \approx 20$ kHz between the central and satellite transitions. Quadrupole splitting is enhanced due to the strain between the Schottky gate and GaAs wafer. The different thermal shrinkages between the GaAs and metal gates enhance the electric-field gradient (EFG) and induce quadrupole splitting, when cooled down to 300 mK. The strain field changes laterally along the quantum well [28]; it has a minimum value right below the center gate, becoming maximum halfway between the center and split metal gate. In this experiment, we apply a negative voltage to the center gate for distributing the electrons in a wide range in space; hence, it is reasonable for the broad ST peak to be separated by approximately 20 kHz from the CT. Our result demonstrates that Δ_f is independent of B, suggesting that the electron channel is located at almost the same position for all B. In addition, this result indicates that our control of V_{CG} and V_{SG} maintains the same QPC channel condition, supporting successful RDNMR.

In Figs. 2(a) and 2(b) another feature of the RDNMR signal can be observed. All the RDNMR signals exhibit broadening. Lowering the magnetic field causes abrupt changes in the diagonal resistance trace, resulting in sharper RDNMR signals. Figure 3(a) shows a representative Gaussian fitting of the RDNMR signal at $B = 1.25$ T obtained using a high-mobility device. For first-order quadrupole interaction, where the quadrupole energy is considerably much smaller than the nuclear Zeeman energy as in this case, the ST linewidth broadening alone is affected, whereas the CT remains unaffected. Thus, to avoid complication, we analyze the FWHM of the CT of both devices, and the results are shown in Fig. 3(b); the red (black) dots indicate the FWHM of the high-mobility (low-mobility) device. The FWHM increases from 4 to 13 kHz on increasing the magnetic field from 1.25 to 7 T with clear saturation in the high-field regime. The FWHM is saturated at 13 kHz, on further increasing the magnetic field.

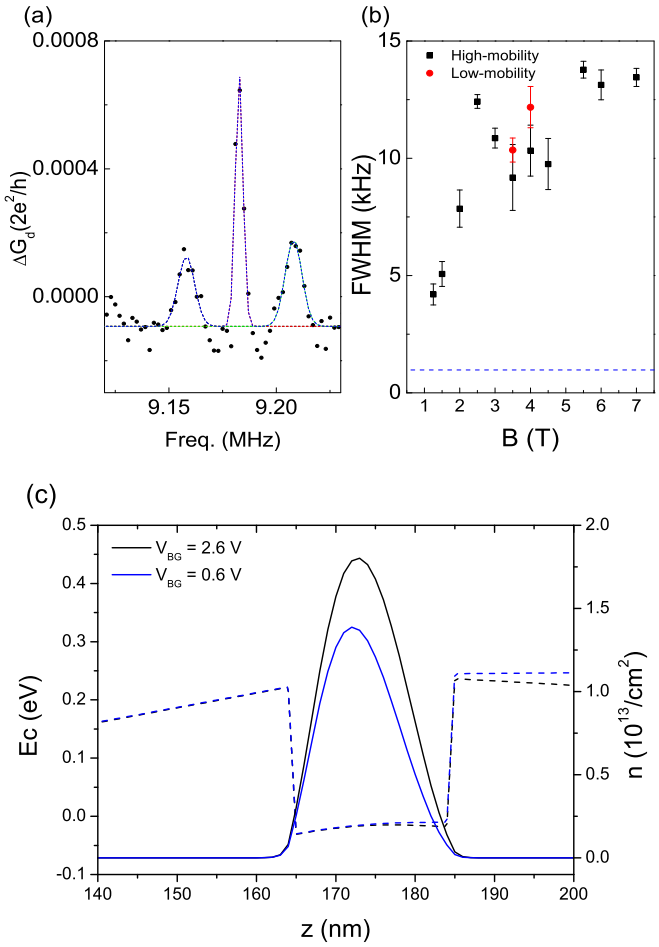

FIG. 3. (a) Representative Gaussian fitting (dashed lines) of the RDNMR signal detected at $B = 1.25$ T using a high-mobility device. Gaussian fitting is used to obtain the FWHM of the central transition. (b) FWHM of the central transition plotted as a function of B. The black dots (red dots) denote the FWHM of the high-mobility (low-mobility) device. The FWHM is dependent on the magnetic field, and approaches a lower limit of 1 kHz (blue dashed lines) corresponding to the nuclear dipole interaction [7,29]. (c) Self-consistent calculation of the conduction band-edge energy and electron density profile along the growth direction, highlighted around the quantum well, for two different backgate bias values.

IV. DISCUSSION

Several factors affect the broadening of the RDNMR signal, namely, dipolar interaction [7,29], quadrupolar interaction [7,14,26], and Knight shifts [12,17,30–33]. The broadening due to direct dipolar coupling (≈1 kHz) is field

independent, whereas the CT is unaffected by quadrupolar interaction. As both interactions are unaffected by B variation, the other interactions should be considered. In nonzero electron spin polarization, the Knight shifts modify the effective Zeeman separation between each state. The Knight shift is proportional to the electron density [$K \propto (n_\uparrow - n_\downarrow)$], which in our case is tuned over the B variation. We can expect the FWHM to increase in proportion with B, when the spatial distribution is maintained constant for the electron channel in the QPC. After changing B, we always tune $\nu_b = 2$ using the backgate voltage. Therefore, to better understand the effect of the bias applied to the backgate, we calculate the out-of-plane electron density distribution in the quantum well using the one-dimensional self-consistent Poisson and Schrödinger equations [34]. The result at $V_{\mathrm{BG}} = 2.6\,\mathrm{V}$ (0.6 V), which corresponds to the V_{BG} applied at $B = 4\,\mathrm{T}$ ($B = 2.5\,\mathrm{T}$), is summarized in Fig. 3(c). The out-of-plane electron density varies slowly with V_{BG} (i.e., the magnetic field); however, this change is very small to explain the FWHM saturation by the variation in the out-of-plane electron density profile. We might need to consider the in-plane electron density distribution to describe the saturation of the FWHM at 13 kHz.

One possible explanation is that the effect of Coulomb interaction compromises the effect of the Knight shifts. Direct Coulomb interaction between electrons is generally characterized by $V_C \propto e^2/\epsilon l_B$. Here e is the elementary charge, ϵ is the dielectric constant, and $l_B = \sqrt{\hbar/eB}$ is the magnetic length. Therefore, the interaction strength scales linearly with the square root of the magnetic field $\sqrt{B}$. The electrons are expected to spread-out spatially with the increase in the field to minimize Coulomb interaction. A recent theory demonstrates that a confined one-dimensional channel changes its shape depending on the magnetic field [35]. It is almost the same without the magnetic field in a low B region, but changes at a high field, reflecting incompressible and compressible stripe characteristics in the IQHE. The transition is expected at a B field where l_B is close to the channel width. Although l_B of approximately 13 nm at 4 T appears smaller than the expected channel width, such a scenario might contribute to FWHM saturation. Further experimental and theoretical studies are needed to clarify this point.

V. SUMMARY

In summary, we detect RDNMR signals under a simplest combination of $(\nu_b, \nu_{\mathrm{qpc}}) = (2, 1)$ down to $B = 1.25\,\mathrm{T}$ ($B = 3.5\,\mathrm{T}$) using a high-mobility (low-mobility) device. The RDNMR amplitude decreases significantly on decreasing the magnetic field. We can deduct the RDNMR observability based on the quality of the $\nu_{\mathrm{qpc}} = 1$ conductance plateau. The RDNMR signal is harder to detect when the $\nu_{\mathrm{qpc}} = 1$ conductance plateau is less pronounced because it reflects the clear separation between the up-spin and down-spin channels. All our RDNMR signals exhibit threefold degeneracy spectra and separation between each peak of $\Delta_f \approx 20\,\mathrm{kHz}$. The splitting is enhanced due to EFG induced-quadrupole interaction, which is independent of the field. On the contrary, the linewidth of the RDNMR signal is dependent on the magnetic field. FWHM analysis reveals that the linewidth broadening is proportional to the magnetic field in a low-field regime reflecting the contribution of the Knight shifts, and saturation at higher fields suggesting the contribution of Coulomb interaction.

ACKNOWLEDGMENTS

We would like to thank K. Muraki of NTT Basic Research Laboratory for supplying high quality wafers for this study. A.N. is supported by a MEXT scholarship for IGPAS student at Tohoku University. K.N. and Y.H. acknowledge support from the Graduate Program in Spintronics, Tohoku University. Y.H. acknowledge financial support from KAKENHI Grants No. 18H01811, No. 15H05867, and No. 15K21727. M.H.F. acknowledge financial support from KAKENHI Grant No. 17H02728.

[1] K. v. Klitzing, G. Dorda, and M. Pepper, Phys. Rev. Lett. **45**, 494 (1980).
[2] B. J. van Wees, E. M. M. Willems, C. J. P. M. Harmans, C. W. J. Beenakker, H. van Houten, J. G. Williamson, C. T. Foxon, and J. J. Harris, Phys. Rev. Lett. **62**, 1181 (1989).
[3] D. A. Wharam, T. J. Thornton, R. Newbury, M. Pepper, H. Ahmed, J. E. F. Frost, D. G. Hasko, D. C. Peacock, D. A. Ritchie, and G. A. C. Jones, J. Phys. C **21**, L209 (1988).
[4] B. J. van Wees, L. P. Kouwenhoven, H. van Houten, C. W. J. Beenakker, J. E. Mooij, C. T. Foxon, and J. J. Harris, Phys. Rev. B **38**, 3625 (1988).
[5] M. Büttiker, Phys. Rev. B **41**, 7906 (1990).
[6] B. J. van Wees, L. P. Kouwenhoven, E. M. M. Willems, C. J. P. M. Harmans, J. E. Mooij, H. van Houten, C. W. J. Beenakker, J. G. Williamson, and C. T. Foxon, Phys. Rev. B **43**, 12431 (1991).
[7] S. Kronmüller, W. Dietsche, K. v. Klitzing, G. Denninger, W. Wegscheider, and M. Bichler, Phys. Rev. Lett. **82**, 4070 (1999).
[8] M. Kawamura, H. Takahashi, K. Sugihara, S. Masubuchi, K. Hamaya, and T. Machida, Appl. Phys. Lett. **90**, 022102 (2007).
[9] W. Desrat, D. K. Maude, M. Potemski, J. C. Portal, Z. R. Wasilewski, and G. Hill, Phys. Rev. Lett. **88**, 256807 (2002).
[10] Y. Hirayama, G. Yusa, K. Hashimoto, N. Kumada, T. Ota, and K. Muraki, Semicond. Sci. Technol. **24**, 023001 (2009).
[11] N. Kumada, K. Muraki, and Y. Hirayama, Phys. Rev. Lett. **99**, 076805 (2007).
[12] L. Tiemann, G. Gamez, N. Kumada, and K. Muraki, Science **335**, 828 (2012).
[13] M. Stern, B. A. Piot, Y. Vardi, V. Umansky, P. Plochocka, D. K. Maude, and I. Bar-Joseph, Phys. Rev. Lett. **108**, 066810 (2012).
[14] M. Kawamura, T. Yamashita, H. Takahashi, S. Masubuchi, Y. Hashimoto, S. Katsumoto, and T. Machida, Appl. Phys. Lett. **96**, 032102 (2010).
[15] K. R. Wald, L. P. Kouwenhoven, P. L. McEuen, N. C. van der Vaart, and C. T. Foxon, Phys. Rev. Lett. **73**, 1011 (1994).

[16] T. Kobayashi, N. Kumada, T. Ota, S. Sasaki, and Y. Hirayama, Phys. Rev. Lett. **107**, 126807 (2011).
[17] M. Kawamura, K. Ono, P. Stano, K. Kono, and T. Aono, Phys. Rev. Lett. **115**, 036601 (2015).
[18] M. H. Fauzi, A. Singha, M. F. Sahdan, M. Takahashi, K. Sato, K. Nagase, B. Muralidharan, and Y. Hirayama, Phys. Rev. B **95**, 241404(R) (2017).
[19] M. H. Fauzi, A. Noorhidayati, M. F. Sahdan, K. Sato, K. Nagase, and Y. Hirayama, Phys. Rev. B **97**, 201412(R) (2018).
[20] H.-M. Lee, K. Muraki, E. Y. Chang, and Y. Hirayama, J. Appl. Phys. **100**, 043701 (2006).
[21] L. A. Tracy, J. P. Eisenstein, L. N. Pfeiffer, and K. W. West, Phys. Rev. B **73**, 121306(R) (2006).
[22] W. Desrat, B. A. Piot, S. Krämer, D. K. Maude, Z. R. Wasilewski, M. Henini, and R. Airey, Phys. Rev. B **88**, 241306(R) (2013).
[23] L. Tiemann, T. D. Rhone, N. Shibata, and K. Muraki, Nat. Phys. **10**, 648 (2014).
[24] A. Singha, M. H. Fauzi, Y. Hirayama, and B. Muralidharan, Phys. Rev. B **95**, 115416 (2017).
[25] Z. K. Keane, M. C. Godfrey, J. C. H. Chen, S. Fricke, O. Klochan, A. M. Burke, A. P. Micolich, H. E. Beere, D. A. Ritchie, K. V. Trunov, D. Reuter, A. D. Wieck, and A. R. Hamilton, Nano Lett. **11**, 3147 (2011).
[26] M. Kawamura, D. Gottwald, K. Ono, T. Machida, and K. Kono, Phys. Rev. B **87**, 081303(R) (2013).
[27] G. Yusa, K. Muraki, K. Takashina, K. Hashimoto, and Y. Hirayama, Nature (London) **434**, 1001 (2005).
[28] M. H. Fauzi, M. F. Sahdan, M. Takahashi, A. Basak, K. Sato, K. Nagase, B. Muralidharan, and Y. Hirayama, Phys. Rev. B **100**, 241301(R) (2019).
[29] T. Ota, G. Yusa, N. Kumada, S. Miyashita, T. Fujisawa, and Y. Hirayama, Appl. Phys. Lett. **91**, 193101 (2007).
[30] G. Sallen, S. Kunz, T. Amand, L. Bouet, T. Kuroda, T. Mano, D. Paget, O. Krebs, X. Marie, K. Sakoda, and B. Urbaszek, Nat. Commun. **5**, 3268 (2014).
[31] N. N. Kuzma, P. Khandelwal, S. E. Barrett, L. N. Pfeiffer, and K. W. West, Science **281**, 686 (1998).
[32] B. A. Piot, W. Desrat, D. K. Maude, D. Kazazis, A. Cavanna, and U. Gennser, Phys. Rev. Lett. **116**, 106801 (2016).
[33] S. Masubuchi, K. Hamaya, and T. Machida, Appl. Phys. Lett. **89**, 062108 (2006).
[34] G. Snider, https://www3.nd.edu/~gsnider/.
[35] P. Armagnat and X. Waintal, arXiv:1903.05028.